OMNY - A tOMography Nano crYo stage

Author(s):
Holler, Mirko; Raabe, Joerg; Diaz, Ana; Guizar-Sicairos, Manuel; Wepf, Roger Albert; Odstrčil, Michal; Shaik, Farooque R.; Panneels, Valérie; Menzel, Andreas; Sarafimov, Blagoj; Maag, Daniel; Wang, Xinyu; Thominet, Vincent; Walther, Hansueli; Lachat, Thierry; Vitins, Markus; Bunk, Oliver

Publication date:
2018-04

Permanent link:
https://doi.org/10.3929/ethz-b-000261046

Originally published in:
Review of Scientific Instruments 89(4), https://doi.org/10.1063/1.5020247

OMNY—A tOMography Nano crYo stage

M. Holler, J. Raabe, A. Diaz, M. Guizar-Sicairos, R. Wepf, M. Odstrcil, F. R. Shaik, V. Panneels, A. Menzel, B. Sarafimov, S. Maag, X. Wang, V. Thominet, H. Walther, T. Lachat, M. Vitins, and O. Bunk

Citation: Review of Scientific Instruments **89**, 043706 (2018); doi: 10.1063/1.5020247

View online: https://doi.org/10.1063/1.5020247

View Table of Contents: http://aip.scitation.org/toc/rsi/89/4

Published by the American Institute of Physics

OMNY—A tOMography Nano crYo stage

M. Holler,[1] J. Raabe,[1] A. Diaz,[1] M. Guizar-Sicairos,[1] R. Wepf,[2,a)] M. Odstrcil,[1] F. R. Shaik,[1] V. Panneels,[1] A. Menzel,[1] B. Sarafimov,[1] S. Maag,[1] X. Wang,[1] V. Thominet,[1] H. Walther,[1] T. Lachat,[3] M. Vitins,[1,b)] and O. Bunk[1]
[1]*Paul Scherrer Institut, 5232 Villigen PSI, Switzerland*
[2]*Scientific Center for Optical and Electron Microscopy ScopeM, ETH Zurich, Zurich, Switzerland*
[3]*EnDes Engineering Partner AG, 4703 Kestenholz, Switzerland*

(Received 21 December 2017; accepted 25 March 2018; published online 13 April 2018)

For many scientific questions gaining three-dimensional insight into a specimen can provide valuable information. We here present an instrument called "tOMography Nano crYo (OMNY)," dedicated to high resolution 3D scanning x-ray microscopy at cryogenic conditions via hard X-ray ptychography. Ptychography is a lens-less imaging method requiring accurate sample positioning. In OMNY, this in achieved via dedicated laser interferometry and closed-loop position control reaching sub-10 nm positioning accuracy. Cryogenic sample conditions are maintained via conductive cooling. 90 K can be reached when using liquid nitrogen as coolant, and 10 K is possible with liquid helium. A cryogenic sample-change mechanism permits measurements of cryogenically fixed specimens. We compare images obtained with OMNY with older measurements performed using a nitrogen gas cryo-jet of stained, epoxy-embedded retina tissue and of frozen-hydrated *Chlamydomonas* cells.
https://doi.org/10.1063/1.5020247

I. INTRODUCTION

Ptychographic x-ray computed tomography (PXCT) is one of many methods for gaining access to three-dimensional internal information of a specimen.[1] With several keV photon energies, it has the potential to bridge the resolution gap between traditional x-ray imaging methods and electron microscopy, imaging in the spatial resolution range approaching 10 nm in high-contrast samples having a thickness of tens of microns.[2,3] Ptychography is a scanning microscopy technique where a sample is illuminated by a spatially confined coherent beam.[4,5] The sample is scanned across the beam such that neighboring illuminated areas partially overlap, and far-field diffraction patterns are recorded for each position. Iterative reconstruction algorithms are used to solve the phase problem and allow reconstructing the 2D complex-valued object transmissivity and the illumination wavefield incident on the sample.[4,6,7] For a 3D sample, this 2D complex-valued transmissivity constitutes a projection of the object along the direction of beam propagation. Much like conventional tomography, a 3D dataset consists of acquiring such 2D projections of a sample along different sample angular orientations with respect to the incident beam propagation. A 3D map can then be reconstructed via computed tomography algorithms.[8] In the case of ptychography, such reconstruction from the phase of the transmissivity leads to a 3D map of the electron density[1] for which the provided contrast is quantitative.[9]

Spatial resolution in x-ray ptychography is neither limited by the step size in the scan nor by the diameter of the illumination, but by the largest angle at which diffraction intensities can be reliably measured. In practice, spatial resolution is also limited by the scanning position accuracy, which within the timeframe of the 2D scan needs to be better than the aimed spatial resolution. To have ptychographic projections result in a high-resolution 3D image, they not only have to provide the required resolution but also have to be distortion free, meaning that not only short-range precision of neighboring scanning positions needs to be accurate but also long-range precision between extreme scanning points. The latter puts strong requirements on thermal drift during the scan and on position distortions, which may be caused by angular error motions of scanning stages or by a small rotation or skewing between the scanning axes and the image pixels. We developed a setup operating at room temperature and atmospheric pressure that can fulfil these strict requirements.[2,10] Exteroceptive laser interferometry is used to measure the relative position between the x-ray beam-defining optics and the sample, which allows accurate position measurements and minimizing thermal drifts. Such metrology has to be compatible with the rotational degree of freedom required for tomography and led to the development of a dedicated tracking interferometer.[11]

This instrument is in routine use, producing valuable scientific results, and recently an isotropic 3D resolution below 15 nm has been demonstrated on an integrated circuit.[3] Such results have been obtained at room temperature in materials relatively insensitive to x-ray radiation. However, there are many systems that suffer from radiation damage, which typically manifests as changes of density and sample deformation.

a)Current address: Centre for Microscopy and Microanalysis, University of Queensland, 4072 St. Lucia, Queensland, Australia.
b)Current address: RUAG Schweiz AG, 8052 Zürich, Switzerland.

Cryogenic sample conditions can alleviate such changes and help us to preserve the sample's structure during the measurement.[12,13] They also enable the measurement of cryogenically fixed specimens and are therefore crucial for many biological applications. Hence various x-ray imaging instruments have been developed exploring various imaging schemes at cryogenic temperatures.[14–18]

One possibility to achieve cryogenic sample temperatures is using a flow of cold gas as often applied in x-ray crystallography. Such a cryo-jet system has also been used with PXCT.[19,20] While cryogenic temperatures can be reached, the relatively uncontrolled gas stream causes drift of the mechanical setup and ice can build up around the sample. Moreover, a gas stream is not compatible with a laser interferometry system[11] because the refractive index changes in the turbulent flow would introduce significant errors in the interferometer measurements that would even prevent interferometry from working at all.

The tOMography Nano crYo (OMNY) stage is the cryogenic variant of the room temperature setup previously described.[2,10] Instead of a free gas-stream, conductive cooling is used to maintain the sample under cryogenic conditions, a strategy akin to that used in cryo electron-microscopy and in other x-ray imaging instruments.[14–17] In order to avoid icing and deposition of material on the sample and other cold surfaces, the setup operates in ultra-high vacuum. The system has a load-lock system for transferring samples to and from the chamber at cryogenic conditions.

OMNY is in operation at the coherent small-angle x-ray scattering (cSAXS) beamline at the Swiss Light Source (SLS) since June 2015 and has been used in various scientific projects already,[13,21–23] therewith demonstrating its functionality: stable cryogenic temperature, small drifts, cryogenic sample transfer, high-precision scanning incorporating rotation, high-resolution 3D imaging, and sample volumes up to 50 000 μm^3. In this article, we describe the OMNY instrument in detail and discuss the performance of the cryogenic and positioning system.

II. BASIC ARRANGEMENT OF THE COMPONENTS OF OMNY

Figure 1 shows the basic components of OMNY. The vacuum chamber is connected via flanges to the beamline (right side) and to an evacuated flight tube (left side) which is used to reduce air scattering and absorption of x-rays when they propagate to the detector after interacting with sample. In all following descriptions, the coordinate system is as follows: z is the direction of x-ray propagation, the x direction is horizontal, and the y direction is pointing up vertically.

Within OMNY, the x-rays first interact with a diffractive x-ray lens[24,25] consisting of a central stop (CS), a Fresnel zone plate (FZP), and an order sorting aperture (OSA). The purpose of this optical system is to provide an x-ray illumination of a few microns in diameter on the sample. The FZP is mounted on a coarse *xyz* stage. This stage system also carries the CS which is mounted on a second pair of *xy* stages in order to align the CS with respect to the FZP. The OSA is mounted on a separate *xyz* stage. Close to the FZP and OSA, there are two flat mirrors

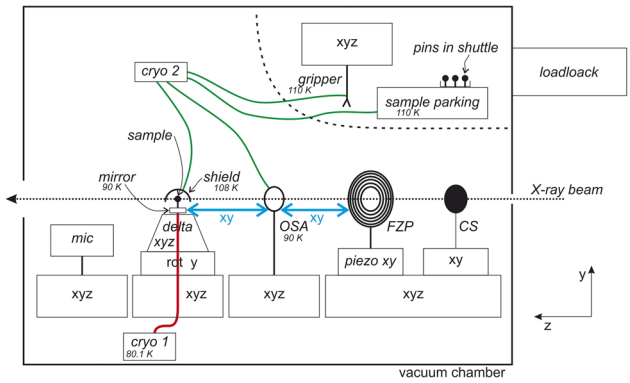

FIG. 1. Schematic overview of the arrangement of components in OMNY. The blue arrows indicate relative interferometric position measurements in the x and y directions, the red line indicates the sample cryogenic system, and the green lines show the peripheral cooling system, as explained in detail in the text. CS: central stop, FZP: Fresnel zone plate, OSA: order-sorting aperture, rot y: rotation stage around the y axis, mic: microscope. The temperature of the cryogenic components is given for each component.

used for a differential interferometric position measurement of the OSA versus FZP in the x and y directions, as indicated by the blue arrows in Fig. 1. The FZP is mounted on a 2D piezo stage (nPoint, Inc., NPXY100D) operated in a closed loop to the measured positions. For alignment of the x-ray optics and samples, an x-ray camera system can be positioned into the beam. FZP optics were chosen for OMNY because of their convenience as they do not require angular alignment and the interferometric measurement of the optics position is simple. With minor modifications, it should be possible to accommodate other optics such as multilayer Laue lenses[26] or compound refractive lenses.[27,28] A Kirkpatrick-Baez mirror[29,30] may be more difficult to implement because of larger dimensions of such a system, which lead to a much higher mass compared to a FZP, and their more stringent requirement of angular alignment and stability.

Just like in the room temperature setup,[2,10] the sample pin[31] is directly mounted on a reference mirror used for the interferometric measurements of the sample position. For the vertical measurement, this reference mirror offers a flat surface, while for the horizontal measurement, it is spherically shaped.[11] This mirror is diamond turned from aluminum and coated with gold (manufactured by LT Ultra GmbH). Having the sample as close as possible to the reference mirror, without any coarse stage in between, is important for precision scanning as this minimizes the interferometer dead-path between the mirror and sample.

The mirror at the sample position is mounted on a home-built piezo scanner[32] based on a delta geometry. The delta scanner is a tripod offering three translational degrees of freedom and it combines a large travel range of 400 μm and high resonance frequency, thereby having a fast speed with a step response <30 ms in typical step sizes of about 2 μm. Compared to the room temperature setup,[2,10] this corresponds to a factor three decrease in positioning overhead. The delta scanner is mounted on a rotation stage and coarse *xyz* stages. The rotation axis is parallel to the y-direction. Two laser interferometers measure the sample position in respect to the OSA in the x and y directions. Another interferometer measures the

rotation of the sample stage's mirror around the beam propagation direction as described in Ref. 2.

Samples are transferred to the chamber using a modified load-lock system based on a VCT100 from Leica Mircosystems. While the main vacuum chamber is pumped by an ion getter pump, the load-lock system is equipped with an additional pumping stage using a turbo molecular pump. This pump is only running during transfer and initial pump-down. Up to six OMNY pins[31] can be transferred in one shuttle to a parking station. A sample gripper[31] is used to mount individual pins in the sample holder, which is machined directly in the reference mirror. Such mounting process can be seen in video 1 of the supplementary material.

The setup is equipped with two cooling systems, as schematically shown in Fig. 1. Cryo 1 is a continuous flow cryostat (Advanced Research Systems, Helitran LT3B). This is an open-loop system featuring low-level vibrations and can be operated with liquid nitrogen or liquid helium. A copper braid is used to connect the cryo-head with the reference mirror of the sample stage. Cryo 2 is a system of pipes going to various places in the vacuum chamber with liquid or cold gaseous nitrogen flowing through. Copper braids are used to transfer heat from various components to heat exchangers installed in the pipe system. The sample parking and the gripper are cooled via the Cryo 2 system. To reduce thermal radiation and contamination of the sample at the measurement position, Cryo 2 also cools the OSA, the OSA holder, and a thermal shield covering the sample during measurements. In OMNY, all mechanical parts are operating at room temperature, and cryogenic components are mounted via insulating structures. To achieve a defined temperature gradient and avoid potential thermal drifts, the room temperature side of each such insulation structures is equipped with a temperature sensor (Heraeus Sensor Technology, Pt 100 C) and a heater (Heraeus Sensor Technology, Pt 6,8 M) operating in closed-loop control. Such heaters are also used at room temperature components that are subject to thermal drift. In these cases, they are simply operated at a temperature a few degrees higher than room temperature for achieving the possibility of active control.

The interferometer positions do not show any difference in the vibration level if the cooling systems are on or off, which indicates low vibration of the cryo-head and sufficient vibration isolation by the copper braid. The instrument is cooled with liquid nitrogen at the beginning of an experimental run and is kept at cryogenic state for weeks. OMNY has thus far not been used for x-ray measurements at room or liquid helium temperatures. In Sec. VIII, we show a detailed evaluation of the performance of the cryogenic setup.

Figure 2 shows the open vacuum chamber with most units installed. The lid of the vacuum chamber, the load-lock system, the vertical interferometers, and the Cryo 2 system are not present in this photograph in order to facilitate the recognizability of the other components. The vacuum chamber is mounted on a block made from mineral cast with dimensions $110 \times 110 \times 52$ cm^3. For the alignment of the rotation axis to the x-ray beam, OMNY is installed on a girder mover system available at the cSAXS beamline. This system offers 3 rotational and two translational degrees of freedom to the entire setup. OMNY is not screwed to this girder system but rests freely on rubber plates for vibration isolation (isoloc Schwingungstechnik GmbH, IPL 10).

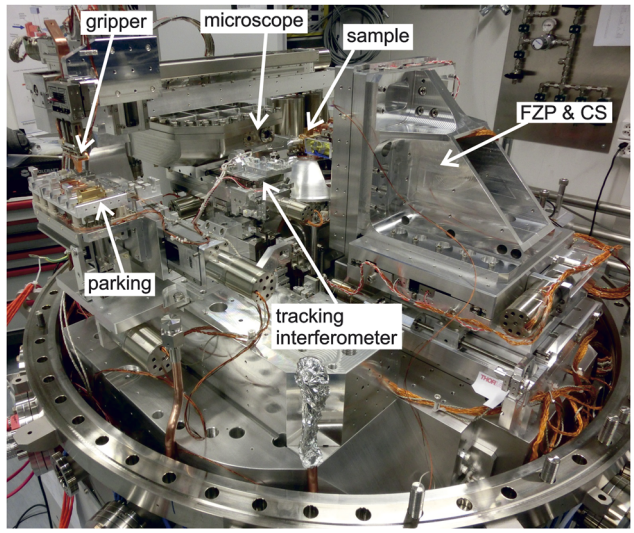

FIG. 2. Photograph of the open OMNY chamber without the laser interferometry and Cryo 2 cooling system installed. The inner diameter of the vacuum chamber is 110 cm. CS: central stop, FZP: Fresnel zone plate.

III. SAMPLE STAGE

The sample stage is depicted in Fig. 3. There are four stepper-motor-driven stages, all using ball-bearings for *xyz* coarse motion and rotation around *y*. The linear stages offer a travel range of ±5 mm. The rotation stage allows a rotation of 365°. A cross section of the components mounted to the rotation stage is shown in Fig. 3(a): the delta stage,[32] i.e., the *xyz* sample scanner, and the cryogenic link system.

The entire mechanical system of stages has a center hole through which the cryogenic link system connects the sample holder, i.e., the reference mirror, to a low-vibration continuous-flow cryostat (Advanced Research Systems, Helitran LT3B). The cryostat is mounted below all the stages. The heat link is created by an oxygen free copper braid with a total length of 514 mm. This copper braid has enough mechanical play and permits the stages to move the required ranges.

As already mentioned, the sample holder is mounted to the delta scanner via a thermal decoupling structure. Mechanically this is a weak component. While translational errors caused by the copper braid are measured interferometrically and then actively compensated, rotational motions around *x* and *y* are not and would cause the 3D spatial resolution to deteriorate. It is therefore important that force and torque generated by the copper braid are transferred to the rotation stage instead of the sample scanner. Such forces are therefore transferred via a sequence of pipes directly to the rotation stage, as shown in Fig. 3(a), and described in more detail in the following.

The cryostat can be operated with liquid helium or liquid nitrogen. In particular, for the case of liquid helium, the available cooling power is limited to approximately 1 W and

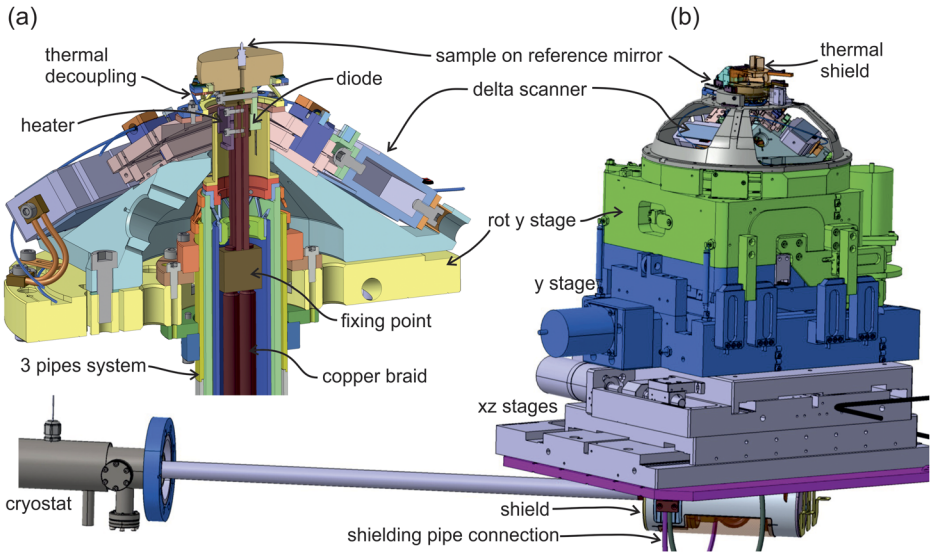

FIG. 3. Sample stage of OMNY. (a) Cross section of the upper region of the sample stage, showing the cryogenic mechanical arrangement in detail. In (b), the full stage system with the cryostat for sample cooling is shown. The total height of this system is 440 mm.

requires proper thermal shielding of the heat link. Therefore, in addition to the copper braid, the cryogenic link system consists of three concentric copper pipes. The outer pipe, depicted in yellow in Fig. 3(a), is directly mounted to the rotation stage and is kept at room temperature. The middle pipe, shown in green, is mounted to the outer pipe via a thermal insulation structure made from polyimide (Vespel, DuPont). This pipe is connected via copper braids to the thermal shield of the cryostat. The inner pipe shown in blue is at cryogenic temperature. It has a diameter of 19 mm and is a mechanical guiding pipe which may get in contact with the copper braid. The braid is mounted to that pipe close to the rotation stage [Fig. 3(a), "fixing point"]. Any force and torque by the copper braid is thus transferred to the rotation stage instead of the sample holder. Below the point where the copper braid is fixed [Fig. 3(a), "fixing point"], there are four individual copper braids each with a cross section of 16 mm^2. Between the connection point and the sample holder, there are 10 individual braids with a total cross section of 23 mm^2 such that the forces caused by the stiffness of the copper braid itself are further reduced.

A heater and a temperature sensor (Cryocon Control Systems, Inc., S950 Silicon diode) are attached to the reference mirror for active temperature control, Fig. 3(a). The heater is built by winding a nichrome wire (Cryocon Part 3039-006) around a copper piece which is fixed with epoxy (Stycast 2850, Catalyst 9). This allows for reasonable heating power even at liquid helium temperatures. All the wires connecting to the cooled sample holder are laid in the inner copper pipe next to the copper braid. Thereby no heat is transferred to the sample holder through the wires, facilitating accurate temperature measurements. The wires leave through the shield at the cryostat and are then wrapped around the cryostat rod and connected to an electrical feedthrough.

The sample holder itself is surrounded by a thermal shield. The open apertures of the shield are kept to a minimum allowing the laser beams of the exteroceptive interferometry[11] to reach the mirror and the OSA to come close to the sample. The shield is connected to Cryo 2, which typically reaches temperatures of 108 K, and it is mounted on a linear actuator (SmarAct GmbH, SLC-1750-S-UHV) such that it can be moved away during sample change (see video 1 of the supplementary material).

The thermal performance of the sample cooling has been modeled with Ansys for the case of operation with liquid helium. From such simulations, a temperature difference of 3.3 K was expected between the cryostat head and the sample holder. Experimentally, a difference of 3.2 K was found such that in a measurement, a temperature of 9.8 K can be achieved at the sample holder. Operated with liquid nitrogen, a stable mirror temperature of 90 K can be achieved with a standard deviation of about 4 mK. Further details can be found in paragraph 7.1.

The delta scanner can be equipped with a local position metrology system.[32] In the present case, this local metrology is based on fiber interferometers (attocube systems AG, Germany) to have nanometric resolution over the entire travel range of the piezo actuators of 450 μm. In order to have this system compatible with the rotation of the sample scanner, the fibers are guided on a spiral along the outer region of the rotation stage's aperture. This prevents the fibers to be bent below their minimum bending radius. Eight revolutions of that spiral permit the 365° of rotation while the change of the diameter of the spiral is within the available space.

IV. X-RAY OPTICS STAGES

The sample stage is mounted on an aluminum base block. On the ($-x$) side of the sample stage, the xyz stage system for moving the OSA is mounted. On the upstream side ($-z$), a relatively large stage system is mounted for the FZP. This stage also carries the central stop (CS) which is installed on an additional xy stage (SmarAct GmbH, SLC-2430-S-UHV). The arrangement is depicted in Fig. 4. The holders of the FZP and OSA are compatible with the gripper mechanism,[31] and special carriers for the load-lock allow transferring these optical elements. It is thus possible to exchange optics even while the system is under vacuum. Figure 4(a) shows the

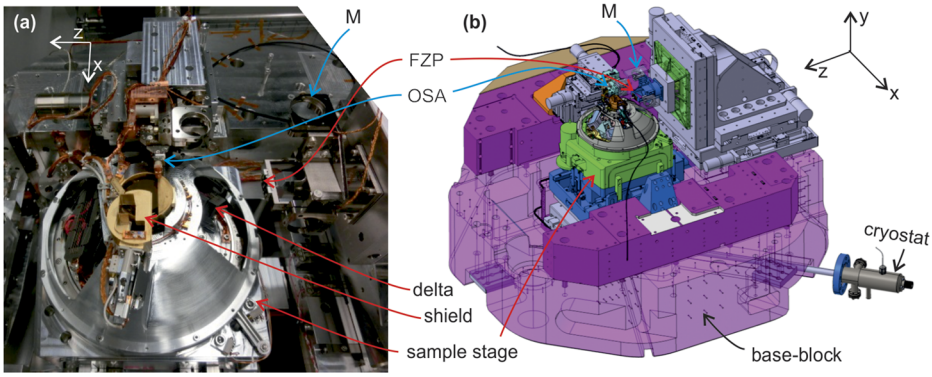

FIG. 4. Sample stage and optics stages on the base block of OMNY. (a) shows a photograph with the thermal radiation shield open and (b) a computer rendering of the design. The width of the purple block is 1 m. Abbreviations: FZP: Fresnel zone plate, OSA: order sorting aperture, M: mirror mount.

mirror mounts (M) for the exteroceptive interferometric position measurement. The OSA holder is connected via an oxygen-free copper braid to the Cryo 2 system, reaching a temperature of 90 K during operation. Thereby the thermal radiation to the sample is minimized as the OSA can be in close distance to the sample.

V. POSITION METROLOGY

The exteroceptive laser interferometry in OMNY is based on hardware from Zygo, Inc. A laser head (model 7714) is used in combination with model 4004 and 2400 interferometer cards. A beam diameter of 3 mm is used. The laser is installed outside the vacuum chamber on the mineral cast and the beam enters the chamber through an optical viewport. The beam is then distributed to all interferometer units using beam splitters. The entire optical system, including the interferometers, is home built. For the position measurements on flat mirrors, a double pass interferometer is used, as described and depicted in Fig. 2b in Ref. 33. In OMNY, the mirrors of the OSA and FZP are mounted on motorized mirror mounts (SmarAct GmbH, STT-25.4-UHV-TI), which enables the fine alignment of interferometers under vacuum conditions and thereby a long term operation of OMNY without opening the chamber.

For the horizontal interferometric position measurement of sample versus OSA, a tracking interferometer[11,33] is used following the reflection from the curved surface of the sample reference mirror in y and z. The continuous alignment of the tracking interferometer is performed in closed loop to a position-sensitive detector and can thus follow the sample reference during sample rotation and linear motion. This continuous alignment of the tracking interferometer results in a synchronized motion of the interferometer with the sample in y and z for which this interferometer is installed on a stack of stages and mounted to the base block. The system is depicted in Fig. 5. From bottom to top, these stages are a vertical stepper-motor-driven linear stage, a horizontal stepper-motor-driven linear stage, and finally a vertical piezoelectric stage (Dynamic Structures and Materials, Custom ZSA-400-PSI Stage). The coarse stages allow an initial alignment of the interferometer. To increase the stiffness of the vertical stage, it is equipped with a piezoelectric brake system.

A ptychographic scan is performed in the xy plane. The continuous synchronized motion of the tracking interferometer and sample therefore requires many movements in the y direction. The vertical piezo stage of the tracking unit offers a range of 400 μm at 200 Hz resonant frequency and is therefore well suited for this task since it has similar properties as the sample scanner.

Because samples are typically not perfectly centered on the sample reference mirror,[11] the mirror wobbles when rotating around the sample during a measurement and requires the tracking interferometer to move in the z direction. A stepper motor is not ideal for this task of continuous closed-loop operation because its response is not very dynamic and would also risk overheating in vacuum. Therefore the horizontal tracking stage is additionally equipped with a second motor, a piezoelectric element for fine motion along the z direction with a 50 μm range. In practice, this range is not sufficient and whenever the piezoelectric element approaches a limit, the stepper motor is activated to move the stage such that the piezo is again centered.

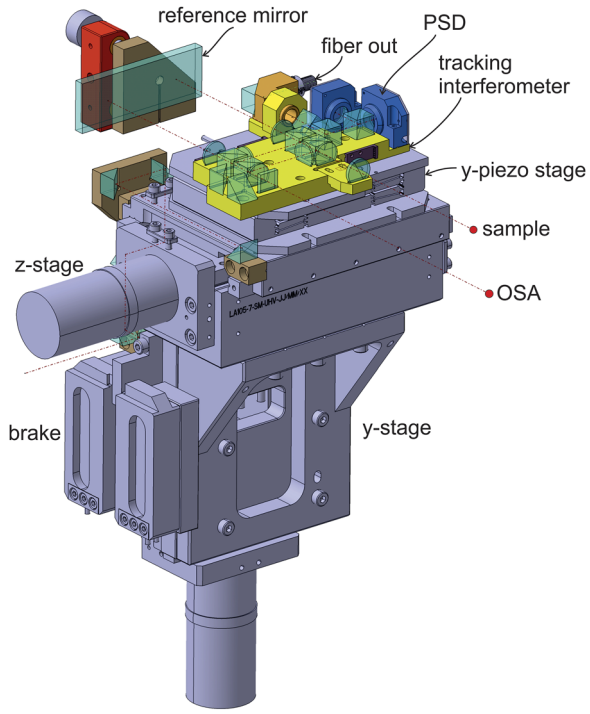

FIG. 5. Tracking interferometer unit of OMNY.

Ptychographic position-refinement algorithms can be used to evaluate the positioning accuracy using strongly scattering test samples. This allows us to test and determine the accuracy of the interferometry and residual errors. See Sec. VIII B for details and experimental data.

VI. MICROSCOPE

OMNY is equipped with an internal optical microscope mounted behind the sample, looking upstream into the x-rays, which offers three different views: (1) a wide angle visible-light camera, (2) an x-ray scintillator for the alignment of x-ray optics and samples, and (3) an optical microscope for alignment of samples as described in Sec. VII. The optical scheme is schematically shown in Fig. 6(a). In the following description, abbreviations in quotation marks refer to elements indicated in Fig. 6(a).

The first optical system offers a wide-angle visible-light overview and is shown in grey in Fig. 6(a), "overview system." This view is useful for seeing inside the vacuum chamber at a perspective that is otherwise not accessible. It is actively used when changing samples in order to supervise the pin insertion process (see video 1 of the supplementary material) and to check for potential mechanical collisions. This system is composed of an objective ("obj," Edmund Optics, Inc., #59-871, 25 mm C Series Fixed Focal Length Lens) and a CCD camera ("cam," IDS Imaging Development Systems GmbH, UI-524xCP-C).

The second optical system has two branches that are combined by a pellicle beam splitter ("p," Thorlabs BP145B1). One branch, shown in red [Fig. 6(a), "x-ray microscopy branch"], is used to acquire x-ray images in transmission. This branch consists of an x-ray scintillator ("sc," Crytur spol.s.r.o., LuAG:Ce, 0.1 mm thickness, polished on both sides) to convert the incident x-rays into the optical regime, a microscopy objective ("o," Mitutoyo, G Plan Apo 20x ref. 378-847 NA 0.28), followed by a camera objective set to infinity ("inf," Stemmer CVO GM310035MCN) and a CCD camera ("cam," IDS Imaging Development Systems GmbH, UI-548xCP-M). This branch offers an optical resolution of 1 μm at the scintillator plane.

The second branch [Fig. 6(a), "visible microscopy branch"] is intended for direct optical imaging of the sample, which can be used for alignment of the sample without the need for x-ray irradiation. While the first branch has its focal plane at the scintillator, the second branch, shown in blue, has its focal plane 66.4 mm in front of the scintillator. It operates at 400 nm wavelength, at which the scintillator is optically transparent, and provides a resolution of 2.5 μm. It consists of a Plan APO ("L1," Leica Plan APO 1.0x WD97—10447176), a zoom objective ("L2," Leica Z16 APO) followed by a camera objective set to infinity ("obj," Stemmer CVO GM310035MCN), and a CCD cameral ("cam," IDS Imaging Development Systems GmbH, UI-548xCP-M). On-axis light for illumination can be achieved using optical-fiber coupling ("f," Leica 10447196).

These components are not UHV compatible. Hence, they are installed in a chamber inside the vacuum system that is at atmospheric pressure. The optical quality of vacuum viewport "w1" has not been specifically selected, but the viewport "w2" contains an optical-quality sapphire window of 3.5 mm thickness. In front of "w2," in the vacuum side, the scintillator crystal is clamp-mounted. All connections are fed through a flexible bellow to the outside and the entire chamber is movable using an *xyz* stage system, shown in Fig. 1. The mechanical stages can be used to switch between the two optical systems and can move the microscope entirely out of the X-ray beam path. Because heat exchange is limited when the chamber is in vacuum, water cooling of the CCD cameras has been implemented by connecting them with copper braids to a water-cooled heat exchanger. The copper braids are not present in Fig. 6.

VII. CONTROL SYSTEM

OMNY is controlled using SPEC (Certified Scientific Software)[34] through OMNY-specific scripts. SPEC controls movements of most stages directly; however, ptychography scans are handled by the real-time control loop which also triggers the detector acquisitions.

The 19 stepper-motor-driven stages in OMNY have been fabricated by Steinmeyer Mechatronik, Dresden, Germany and are controlled by three motor controllers from Galil Motion Control (DMC-4080-D4140). The stages are equipped with encoders (Renishaw Tonic UHV). The motor controllers run custom software for limiting the following error, i.e., the error of step and encoder position, for motor temperature supervision, for closed-loop motion control to the encoder positions, and for the automatic extension of the travel of the tracking piezo stages by repositioning stepper-motor-driven stages.

The six piezo-driven stick-slip stages (SmarAct) are controlled by their corresponding SmarAct MCS controller. The sample temperature is controlled by a Cryocon 24C

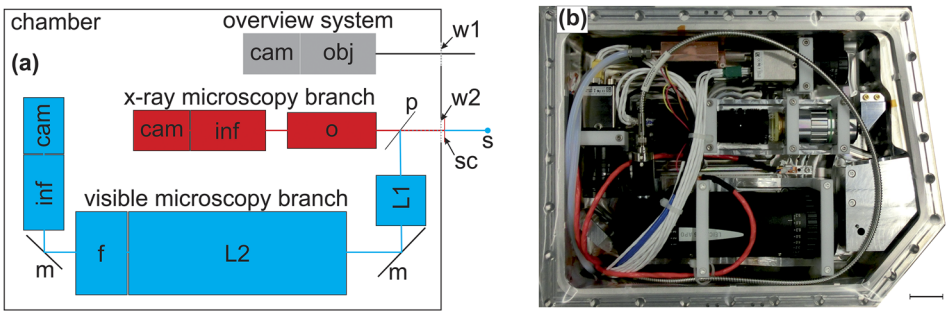

FIG. 6. Microscope of OMNY. (a) Schematic arrangement of the optical components, where abbreviations are described in the text. (b) Photograph of the x-ray eye with the same orientation, scale bar 25 mm.

temperature controller. The other heater/temperature sensors are interfaced to home-built amplifier electronics equipped with temperature controllers from OMEGA Engineering, Inc.

For the real-time control of OMNY, there is one central host PC running Ubuntu Linux with a real-time kernel (RTAI 4.0). A real-time control loop manages closed-loop motion and scanning. This PC also runs several soft-IOC (input output controller) to provide EPICS (Experimental Physics and Industrial Control System)[35] channels dedicated to keep track of the sample names and their positions in the parking or sample holder, temperatures of the instrument, and status and control of the vacuum system.

The real-time loop controls the piezoelectric elements of the delta scanner and tracking interferometer in a closed loop to the measured position data, and it performs the ptychography scans. The loop is schematically shown in Fig. 7 and operates at 2.5 kHz. Communication with SPEC is achieved via an ethernet interface that communicates asynchronously with the real-time control loop. The modules that exchange information with SPEC are depicted in yellow.

Interferometer data are provided by a model 4004 and 2400 interferometry card from Zygo, Inc. These cards are based on the versa module europa (VME) bus and are interfaced to the PC using a VME64-to-Peripheral Component Interconnect (PCI) bus-to-bus adapter (Abaco Systems, model 810). Various PCI cards from National Instruments are used to get access to other signals and to control the hardware: A model 6259 is used for analog input and output (2 voltage channels), a model 6733 is used for analog output (8 voltage channels) and a 6602 counter card is used to read and decode the quadrature encoder signals from the attocube interferometer unit used as local metrology in the delta sample positioning unit.

All piezoelectric stages are controlled by analog voltages. For the fast positioning of the delta scanner, the voltage amplifier has to provide high current. We achieve a current of 1 A using a VF-500 amplifier from Dynamic Structures and Materials, LLC. However, high current piezoelectric amplifiers typically have high noise levels, which, given the large travel range of 450 μm of the delta scanner, would introduce position noise around 10 nm. To circumvent this problem, the piezoelectric stacks in the delta scanner are split into four with independent wiring, and only one of these stacks is driven with the high-current amplifier, thereby reducing the position noise but also the travel range. The remaining stack is driven by a low-noise and low-current amplifier (model SVR-150 from Piezomechanik Dr. Lutz Pickelmann GmbH). In this manner, closed loop sample stability below 10 nm standard deviation can be achieved (see also Fig. S1 of the supplementary material).

The vertical and horizontal tracking piezoelectric stages are controlled by the low-current amplifier SVR-150. The FZP Npoint piezoelectric stage is controlled by an Npoint LC.403 controller.

Similar to the room temperature setup,[2,10] the sample reference mirror, which serves as sample holder, is diamond turned from aluminum and coated with gold (manufactured by LT Ultra GmbH). The resulting long-range shape errors are

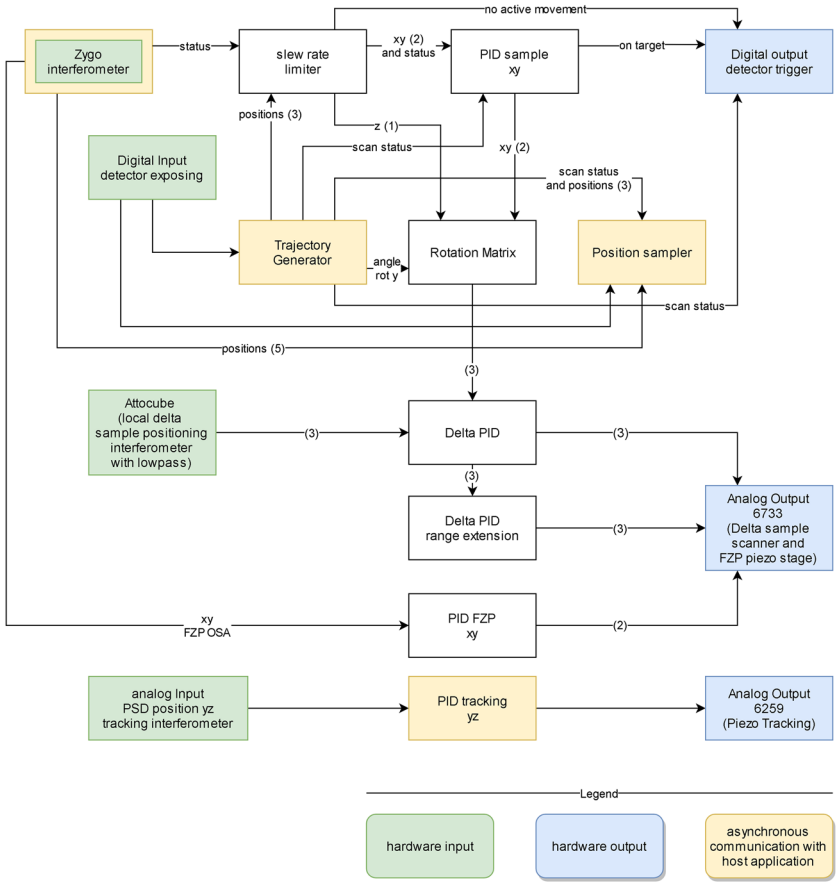

FIG. 7. Schematic of the real-time control system loop. Hardware input modules are shown in green, output modules in blue, while modules communicating with the host computer are shown in yellow. The arrows indicate the information flow between the modules and the number in brackets corresponds to the number of channels active in these connections.

below 300 nm, while the surface roughness is in the 1 nm range. Since the sample is directly mounted on this mirror, it can only be centered to the symmetry axis of the mirror sphere equator to within 50-100 μm.[11] During operation, the delta scanner runs in closed loop to the exteroceptive interferometer signal. Therefore, sample alignment effectively means determining the sample offset, which depends on the rotation angle, and shifting the field-of-view (FOV) accordingly. Once calibrated, the surface shape errors can be in principle compensated for in the measurement. However, because the fine alignment of the projections is based on image processing[36] and the shape error of the mirror is negligible in the measurement, the aforementioned compensation during measurement is not essential. The interferometry mainly assures high-resolution and distortion-free projections that are subsequently aligned on the nanometer level in a post-processing step.[2,36,37]

For data acquisition, samples are aligned in a two-step process. First the sample is aligned based on camera images of the x-ray eye (see Sec. VI) and using a graphical user interface developed in LabView (National Instruments Corporation) which interacts directly with SPEC. Camera alignment requires finding the relative position between the FZP and the sample at five different rotation angles evenly spaced and ranging from 0° to 180°. Based on this initial alignment, a fine alignment step is performed using ptychography in which five ptychographic scans are performed based on the positions obtained with the x-ray eye. The ptychography reconstructions provide better spatial resolution and sensitivity and allow a more precise selection of the outer contour of the sample at each angular position and further allow for tighter margins around the sample volume. With five alignment positions, a reliable sinusoidal curve fit can be performed and subsequent ptychography scans for the acquisition of the full tomographic dataset are shifted in position accordingly.

The Zygo interferometers measure five positions exteroceptively: *xy* of the sample versus OSA, *xy* of OSA versus FZP, and the rotation angle around *z* of the sample stage. The *xy* position data of FZP versus OSA are directly fed to proportional integral differential (PID) control loops (denoted "PID FZP *xy*" in the sketch in Fig. 7) which generate the required output signal to keep the relative position between these elements stable in closed loop. Because this is not a high-frequency signal, it mainly compensates slow drifts.

For the *xy* control of the sample position, a trajectory generator module creates target positions in *xyz*. This module can move the sample to a single requested position or handle an entire sequence of positions, i.e., a scan, by either computing the next position based on provided parameters or by running through an array of previously stored positions. The module can handle point-by-point scans or continuous trajectories for on-the-fly ptychography.[38–40]

During x-ray exposures, a sampler module records the position data of all five axes of the Zygo interferometers and computes mean and standard deviation for each point of the scan. This module can be read out after the scan and the data can be used in the ptychography reconstruction algorithm.

The *xyz* positions of the sample versus OSA are fed to a slew-rate limiter in order to prevent sudden large movements which may not be followed successfully by the tracking interferometer and thereby risk losing the interferometer signal. The slew-rate limiter compares the new target positions with the current position and if the step is larger than 10 μm, it creates a smooth and slower trajectory. Additionally, it receives and monitors status information from the Zygo interferometers. If the signal strength of the tracking interferometer decreases below a threshold, it will momentarily stop the motion of the sample stage to wait for the tracker. The output positions of the slew-rate limiter are fed to a PID loop (denoted "PID sample *xy*" in Fig. 7) that generates the required output corrections for accurate positioning. The output of the closed-loop *xy* signals from this module as well as the *z* position of the slew-rate limiter is fed to a rotation matrix module that adapts the PID outputs to the geometry of the delta stage.

The three axes of the delta scanner are perpendicular to each other but mounted in a rotated geometry with respect to the OMNY coordinate system such that the three axes are like the sides of a cube hanging from one corner. To achieve a given *xyz* sample position, the rotation matrix module computes the required output for the three axes of the delta stage. These positions are fed to the PID controller of the delta positioner, which compares the target positions with the current position of each axis as measured with the local metrology, i.e., the attocube interferometers. The output of this PID module is directly fed to an analog output module to which the high-current piezoelectric amplifiers connect. Additionally the output signal of the PID module it is fed to the slow PID controller of the delta stage. The latter constantly re-centers the fast piezo to the middle of its range such that fast movements can be performed in any direction at all times. The slow PID module generates the analog voltages for the slow piezoelectric stack of the delta scanner.

VIII. OPERATION AT THE BEAMLINE AND MEASUREMENT PERFORMANCE

OMNY is operated at the cSAXS beamline at the Swiss Light Source (SLS), Paul Scherrer Institut, Switzerland. The initial pump-down of the chamber is done using the turbo molecular pump of the load-lock. After a week, the ion-getter pump is started. After another week, a pressure of 1×10^{-7} mbar is reached and the pump of the load-lock is separated from the chamber by the load-lock valve and switched off. Although the setup could be baked at 100 °C, a bake-out has never been performed with OMNY. The pump-down is not done at the beamline, instead the setup is brought to the beamline fully assembled and already under vacuum using the crane of the SLS experimental hall; the full weight of OMNY is 4 metric tons. Once at the beamline, the cryogenic system is connected and the cool-down takes about 3 h. As mentioned earlier, thus far measurements in OMNY were always done with liquid nitrogen cooling. Liquid helium has been used for testing the cryo system but never for an x-ray measurement. OMNY has also never been used to measure at room temperature. At cryogenic temperature, the pressure of the vessel is further reduced to 2×10^{-8} mbar. Once pumped and in operation the setup is kept under vacuum and at cryogenic temperature for the entire OMNY experimental run, which

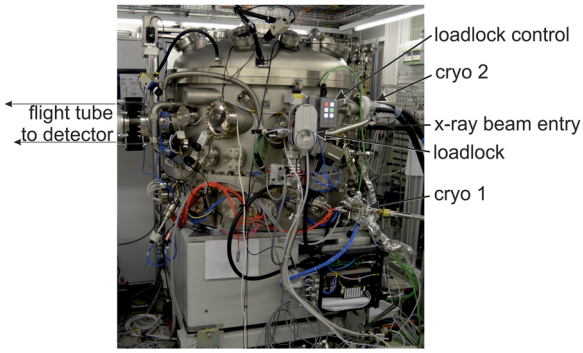

FIG. 8. Photograph of OMNY installed at the cSAXS beamline at SLS.

typically lasts 5–6 weeks. The flight tube that is attached to OMNY only reaches a pressure of 10^{-3} mbar, which is why OMNY is separated from the flight tube by a 13 μm thick Kapton foil. For fast cabling, there are cabling boxes installed that are equipped with high-density industrial connectors from ODU and Harting. Such connectors have the robustness for frequent moves of the setup, simplify commissioning, and reduce re-cabling time significantly. The connectors are mechanically encoded such that false connections are not possible. Figure 8 shows a photograph of OMNY at the cSAXS beamline.

The x-ray beam at cSAXS is generated by an in-vacuum undulator with 19 mm period.[41] The vertical source size is 20 μm. Horizontally a secondary source is defined by a slit, 12.1 m downstream of the undulator. The slit is set to 20 μm width in order to have a spatially coherent illumination of the FZP in OMNY. Temporal coherence is achieved by a Si(111) double-crystal fixed-exit monochromator in combination with a fused silica mirror suppressing higher harmonics.

A. Performance of the cryogenic system

Figure 9(a) shows the temperature evolution of the sample stage over the duration of a 5 day user experiment. The average temperature is 90.000 K with a standard deviation of 3.3 mK. This temperature stability is kept throughout an OMNY experimental run, which typically lasts 5–6 weeks. Similarly, other components are required to maintain cryogenic conditions. Figure 9(b) shows the corresponding temperature of the gripper, the OSA holder, the sample parking, and the sample shield. While cryogenic temperature is also well maintained, the temperature fluctuates more compared to the sample stage because the former components do not have a heater installed for temperature stabilization. Instead a heater is placed at the room-temperature parts to achieve low-drift conditions and well-defined temperature gradients over the insulating structures.

B. Positioning accuracy, stability and drift

For a scanning x-ray microscope such as OMNY, accurate sample positioning is crucially important. Here three quantities are of main interest: position stability during exposure, positioning accuracy, and long term drift. The long term drift in OMNY is determined mainly by temperature drifts of critical components such as the sample mirror. As can be seen in Fig. 9(a), the temperature stability of the sample stage is excellent, with a standard deviation of a few mK. Room temperature components such as the FZP are heated to slightly above room temperature to achieve stable conditions. Due to this heating mechanism, long-term drift is much smaller compared to the previous setup which operates at room temperature and atmospheric pressure, which does not have any temperature control.[10] However, even in the previous setup, long-term drifts of a few 100 nm/day have never been a limitation for x-ray ptychographic nanotomography. Because we use post-processing alignment, as described in more detail below, drifts only play an important role if they are larger than the target resolution within the time-frame of measuring a 2D projection, which is currently on the order of a minute. The long-term drifts should then be only good enough to have the samples remain within the measurement field of view, which is reliably achieved.

In order to achieve non-distorted reconstructions that are consistent among each other and can be combined to a high-quality tomogram, positioning accuracy is important. Since raw interferometer data may contain systematic errors, it is preferable to use an independent method to estimate sample positions and investigate their effects on the performance in a ptychographic measurement. Since position refinement algorithms can provide precision in order of nanometers in X-ray ptychography,[42,43] provided that the sample has sufficiently high contrast, such algorithms can be used to diagnose and characterize the errors of the laser interferometry.

For this purpose, we use the 2D test pattern that was already used in the room-temperature setup.[2] This sample was fabricated using 100 keV electron beam lithography in hydrogen silsesquioxane (HSQ) on a Si_3N_4 membrane. The smallest feature size on the Siemens star is 10 nm and the

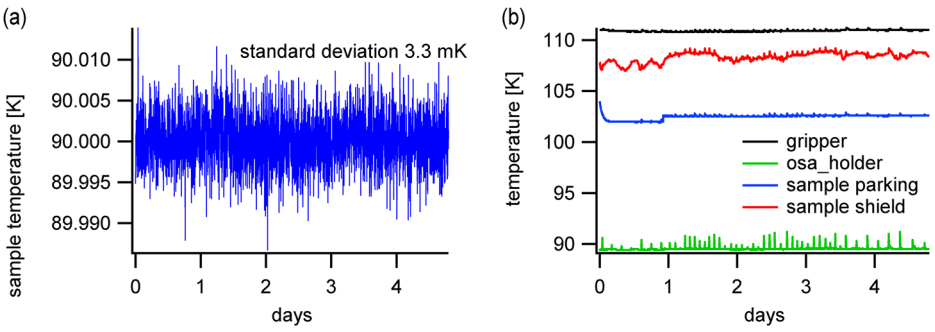

FIG. 9. (a) Temperature of the sample stage measured over 4.8 days showing a standard deviation of 3.3 mK. (b) Corresponding temperature of various cryogenic components: the gripper, OSA holder, sample parking, and sample shield.

height of the HSQ is 700 nm. The sample was coated with a 10 nm thick layer of iridium using atomic layer deposition. A detailed description of the preparation of similar samples has been published elsewhere.[44]

Two independent scans of a 5 μm × 5 μm region have been performed at cryogenic temperature with positions following a Fermat spiral trajectory[45] with an average step of 0.5 μm and an exposure time of 0.1 s/position. Diffraction patterns were recorded using a Pilatus 2M detector[46] positioned at a distance of 7.33 m. For reconstruction, we used the central 1408 × 1408 pixel region which results in a reconstruction pixel size of 6.0 nm.

For undistorted reconstructions, the interferometry axes are ideally mutually perpendicular and are aligned with the detector pixels. The setup alignment procedures presented earlier[2] are also applied in OMNY such that the axis of rotation is perpendicular to the incoming X-ray beam and the detector pixels are well aligned to the axis of rotation. However, this procedure does not guarantee alignment of the interferometry to the detector pixels. During commissioning of OMNY, an affine correction matrix is determined using the "flipping experiment" described in Ref. 2 and then performing a search of the matrix parameters that provide the reconstructions with highest FSC (Fourier shell correlation) resolution estimates.[47] This procedure is only done once at the beginning of an OMNY run and the resulting matrix is used to correct the positions provided to the ptychography reconstruction algorithm for all subsequent measurements of the experimental run.

For characterizing the positioning errors, in this case, we first independently determined for a pair of identical scans the affine correction matrix

$$\begin{pmatrix} x_{\text{corrected}} \\ y_{\text{corrected}} \end{pmatrix} = \begin{pmatrix} 1 & 0.0072 \\ 0.0012 & 1 \end{pmatrix} \begin{pmatrix} x_{\text{measured}} \\ y_{\text{measured}} \end{pmatrix},$$

using global-parameter position refinement with the LSQ-MLc algorithm,[42] this provides information about systematic errors introduced by misalignment of the interferometer arms with respect to the transverse orientation of the detector pixels. The corrected positions are then used for the ptychographic reconstruction. The measurement of the 2D test pattern was reconstructed using 1000 iterations of the LSQ-MLc method[42] with and without position refinement and sub-pixel shifts of the illumination probe.

Figure 10(a) shows the reconstructed phase image with the positions of the scan indicated by circles. The arrows indicate the estimated position corrections for each scan determined by the position refinement method, note however that the position error magnitude shown is scaled up by a factor 20. The position errors determined are plotted for both axes in Figs. 10(c) and 10(b) that show a zoom to the central region of the reconstruction, with and without the position refinement step, showing that the quality improvement due to position refinement is almost negligible for this dataset. The residuum between the original interferometry positions and the refined ones shows a strong correlation of the position errors between the two subsequent scans. The standard deviation of

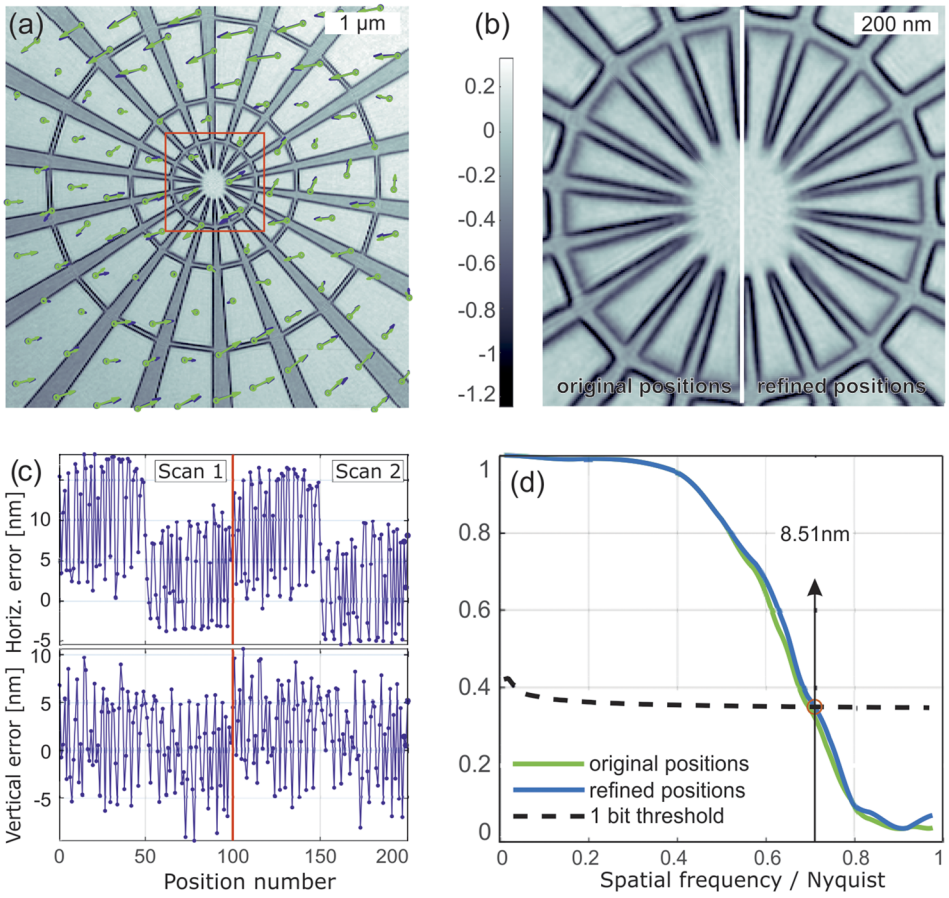

FIG. 10. Positioning accuracy and stability in OMNY. (a) Phase reconstruction of a 2D test object with circles indicating the scan positions and arrows showing the computational position corrections. Blue and green show the results for scan 1 and scan 2, respectively. The magnitude of the arrows was up-scaled by a factor of 20. (b) Zoom of the central region showing the reconstruction with the original positions derived from interferometry data compared to that after position refinement. (c) Horizontal and vertical position errors for both scans in nm. (d) Intersection of the Fourier shell correlation curve with the 1-bit threshold curve indicates imaging reproducibility down to 8.5 nm for the reconstruction with position refinement and 8.7 nm for the reconstruction with interferometer positions.

the residues is 8.1 nm and 4.7 nm in the horizontal and vertical directions, respectively. The standard deviations of the random errors, i.e., the difference between refined positions from both scans, were 1.8 nm and 2.4 nm in the horizontal and vertical directions, respectively. The reproducibility of the two ptychography reconstructions was evaluated using Fourier ring correlation (FRC).[47] The FRC curve [Fig. 10(d)] intersects the 1-bit threshold, indicating a half-period resolution of each of these images of 8.5 nm for a reconstruction with position refinement and at 8.7 nm using the original interferometry positions. The complex-valued illumination probe is depicted in Fig. S2 of the supplementary material.

For each scanning point, the control system also computes the standard deviation of the sample with respect to the probe position during exposure (Fig. 7, position sampler). The corresponding plot in Fig. S1 of the supplementary material shows that the in-position stability of OMNY in the presented measurements is only slightly below 10 nm in average. Thus the achieved image resolution of 8.7 nm matches the mechanical vibration level of OMNY. Such high-resolution should not be expected in case of low-contrast biological samples. The best 3D resolution demonstrated on a biological, but strongly scattering sample was 27 nm on a beetle wing scale.[13]

C. Measurement performance for low-contrast biological material

Prior to OMNY, Ptychographic x-ray computed tomography at cryogenic conditions was performed using a setup of stacked commercial components with a cold nitrogen gas (cryo-jet) blowing at the sample.[19,20] This setup was not compatible with exteroceptive position metrology and suffered from large thermal drifts which deteriorated the spatial resolution and made measurements troublesome because ice could build up on the sample or the sample could even drift out of the field of view. In Ref. 19, results obtained using that setup on frozen-hydrated *Chlamydomonas* cells were presented, for which the data acquisition took about 13 h. In Fig. 11(a), we show a single slice of about 44 nm thickness through the reconstructed tomogram, revealing some high-density spherical organelles inside the cell identified as polyphosphate bodies (PB),[48] starch platelets (SP) forming a closed structure around the pyrenoid (P) and some other starch granules (S) scattered within the cell.[19] In this experiment, the half-period resolution was about 206 nm (see Fig. S3 of the supplementary material) in 3D limited by distortions in 2D projections mainly caused by thermal drifts.

Chamydomonas cells are frequently used for demonstrating bioimaging with X-ray microscopy,[49,50] and thus we repeated the measurement in OMNY using a photon energy of 6.2 keV, identical to that used in our previous experiment.[19] Details about sample preparation and measurement can be found in the supplementary material. For this measurement, data acquisition took about 10.5 h and a 3D half-period spatial resolution of 111 nm was estimated in the tomogram by Fourier shell correlation (see Fig. S3 of the supplementary material). Next to better spatial resolution, measurements with increased position accuracy afforded by OMNY are also characterized by lower noise because of improved consistency in the object-space overlap constraint.[6] In Fig. 11(b), we show a single slice through a cell of the tomogram acquired with OMNY. Compared to the previous measurement shown in Fig. 11(a), some polyphosphate bodies (PB), starch platelets (SP), and starch granules (S) are also visible inside the cell. Moreover other organelles can be clearly distinguished: the pyrenoid (P) with a different density, surrounded by starch platelets (SP), the cell wall (CW) surrounding the cell, and a faint but visible organelle inside a slightly lower-density area in the center of

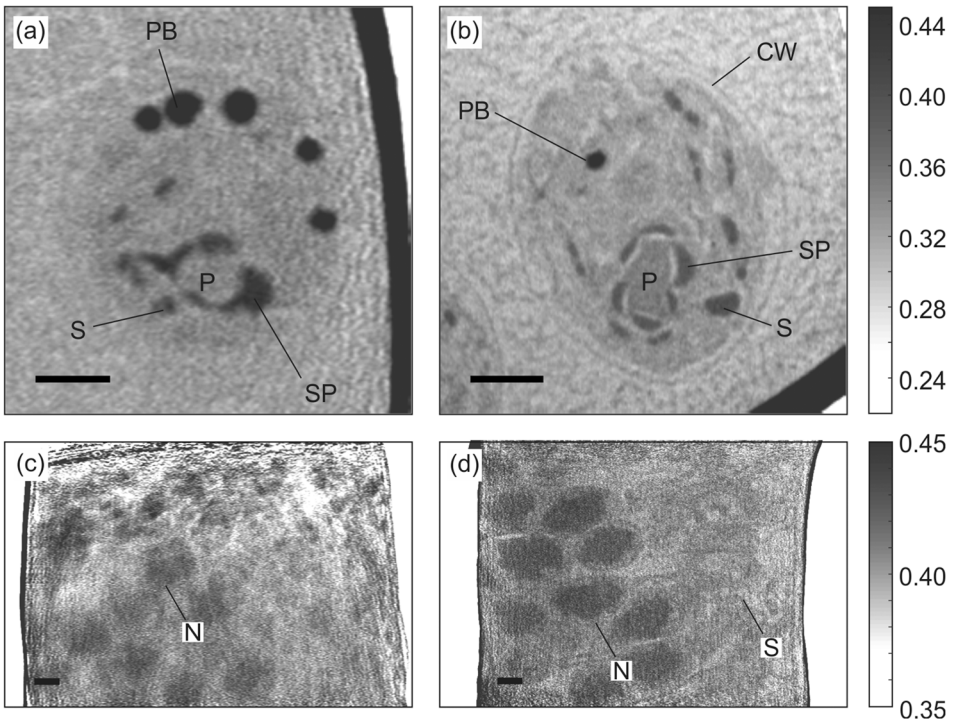

FIG. 11. Comparison of imaging results with a cryo-jet-based setup without exteroceptive metrology[11] [(a) and (c)] and OMNY [(b) and (d)]. The grayscale indicates electron density (e–/Å3). Samples correspond to frozen-hydrated *Chlamydomonas* cells [(a) and (b)] and epoxy-embedded stained retina tissue [(c) and (d)]. All measurements were recorded at 6.2 keV photon energy. Scale bars are 2 μm. In (a) and (b), the pyrenoid (P), starch granules (S), polyphosphate bodies (PB), starch platelets (SP), and cell wall (CW) are indicated. In (c) and (d), the cell nuclei (N) and synaptic terminals (S) are marked.

the cell may correspond to the nucleoid inside the cell nucleus although the nuclear membrane is not resolved. However, the granular structure which is now observed outside the cell indicates that there might be ice crystals in the sample which could have formed due to an insufficiently rapid freezing by plunging in liquid ethane. In fact, the diameter of the capillary at the position of the cells is about 20 μm in diameter in both samples and would be consistent with such limitation in cryogenic sample preparation.

We suspect that the observable cell structures in the present measurement were altered by water crystallization: For instance, the shape of cell walls (CW), pyrenoid (P), and starch platelets (SP) deviates significantly from the more rounded shapes they exhibit in high-pressure frozen specimens[31] or in plunge frozen specimens immersed in a thin layer of water without a glass capillary.[41] Such artifacts were not observed in frozen-hydrated tissue samples measured with OMNY[21] that were directly mounted on a Cu OMNY pin[31] and heavily infiltrated with cryogenic-protectant.

Another example of an earlier measurement performed with a cryo-jet is shown in Fig. 11(c). In this case, the sample was a pillar of 20 μm diameter of an epoxy-embedded stained retina tissue. A tomogram was acquired over a period of 13 h, of which we estimate the 3D spatial resolution to be 755 nm, as detailed in the supplementary material (see also Fig. S3). The image corresponds to an orthoslice of the tomogram with a thickness of a single voxel, which corresponds to 31.6 nm. In addition to thermal drifts, other experimental problems occurred during the measurement. On the top part of the image, there are many artifacts due to the formation of ice during the acquisition, which caused problems not only in the ptychographic imaging of individual projections but also in the alignment of projections needed for high-resolution nanotomography.[36] The measurement of a similar specimen with OMNY provided much better results as shown in the orthoslice in Fig. 11(d). In this case, the measurement took about 16.6 h and the estimated 3D spatial resolution is 152 nm (see Fig. S3 of the supplementary material). Both slices in Figs. 11(c) and 11(d) correspond to a region of the retina tissue where both cell nuclei (N) and synaptic terminals (S) are present. Due to the poor quality of the cryo-jet experiment, only cell nuclei, of approximately 2 μm size, are visible in Fig. 11(c). Only the later measurement with OMNY revealed both types of structures, Fig. 11(d). Details about the samples, their preparation and measurements can be found in the supplementary material.

The contrast in all these samples is very weak and therefore it is difficult to reach high spatial resolution.

IX. SUMMARY AND OUTLOOK

We presented the OMNY instrument in detail. In addition to the mechanical arrangement, the sample stage with its cryogenic heat link and the control of the instrument has been described.

While OMNY already provided high spatial resolution images at cryogenic conditions in polymer[23] and biological samples,[13] we believe that it can become a unique tool for visualizing frozen hydrated specimens in 3D. The instrument has proven to provide sub-30 nm 3D resolution in high-contrast specimens[13] at cryogenic temperatures and will be useful to explore the limits in resolution achievable in frozen-hydrated specimens. For example, while sub-20 nm resolution has been demonstrated in frozen-hydrated cells in 2D,[50] we should now be able to find out if such spatial resolution can also be achieved in 3D. Additionally, OMNY's capability to cool to temperature of ~10 K allows for investigations whether such reduced temperatures help us to further alleviate radiation damage.

The exit window at the end of the evacuated flight tube is a Mylar foil with 300 μm thickness. This foil produces a considerable amount of scattering and absorption which deteriorates the data quality. It is therefore foreseen to switch to an in-vacuum detector permitting recording data with a lower background noise in the near future.

SUPPLEMENTARY MATERIAL

See supplementary material for V1 Video of a sample mounting in OMNY. Most views correspond to the actual camera view that is available to the operator. Some parts were recorded when not all components of OMNY were installed and the chamber open.

ACKNOWLEDGMENTS

This work was supported by the SNF R'Equip (Project No. 145056) and the Competence Centre for Materials Science and Technology (CCMX) of the ETH-Board, Switzerland. Ptychography data were collected at the coherent small-angle x-ray scattering (cSAXS) beamline at the Swiss Light Source at the Paul Scherrer Institut in Villigen, Switzerland.

[1] M. Dierolf *et al.*, "Ptychographic x-ray computed tomography at the nanoscale," Nature **467**, 436–439 (2010).
[2] M. Holler *et al.*, "X-ray ptychographic computed tomography at 16 nm isotropic 3D resolution," Sci. Rep. **4**, 3857 (2014).
[3] M. Holler *et al.*, "High-resolution non-destructive three-dimensional imaging of integrated circuits," Nature **543**, 402 (2017).
[4] P. Thibault *et al.*, "High-resolution scanning x-ray diffraction microscopy," Science **321**, 379–382 (2008).
[5] J. M. Rodenburg *et al.*, "Hard-x-ray lensless imaging of extended objects," Phys. Rev. Lett. **98**, 034801 (2007).
[6] M. Guizar-Sicairos and J. R. Fienup, "Phase retrieval with transverse translation diversity: A nonlinear optimization approach," Opt. Express **16**, 7264–7278 (2008).
[7] P. Thibault and M. Guizar-Sicairos, "Maximum-likelihood refinement for coherent diffractive imaging," New J. Phys. **14**, 063004 (2012).
[8] A. C. Kak, M. Slaney, and G. Wang, "Principles of computerized tomographic imaging," Med. Phys. **29**, 107 (2002).
[9] A. Diaz *et al.*, "Quantitative x-ray phase nanotomography," Phys. Rev. B **85**, 020104 (2012).
[10] M. Holler *et al.*, "An instrument for 3D x-ray nano-imaging," Rev. Sci. Instrum. **83**, 073703 (2012).
[11] M. Holler and J. Raabe, "Error motion compensating tracking interferometer for the position measurement of objects with rotational degree of freedom," Opt. Eng. **54**, 054101 (2015).
[12] M. R. Howells *et al.*, "An assessment of the resolution limitation due to radiation-damage in x-ray diffraction microscopy," J. Electron Spectrosc. Relat. Phenom. **170**, 4–12 (2009).
[13] B. D. Wilts *et al.*, "Evolutionary-optimized photonic network structure in white beetle wing scales," Adv. Mater. **2017**, 1702057.
[14] A. Sorrentino *et al.*, "MISTRAL: A transmission soft x-ray microscopy beamline for cryo nano-tomography of biological samples and magnetic domains imaging," J. Synchrotron Radiat. **22**, 1112–1117 (2015).

[15]S. Chen *et al.*, "The bionanoprobe: Hard x-ray fluorescence nanoprobe with cryogenic capabilities," J. Synchrotron Radiat. **21**, 66–75 (2014).
[16]G. Schneider *et al.*, "Three-dimensional cellular ultrastructure resolved by x-ray microscopy," Nat. Methods **7**, 985–987 (2010).
[17]E. Nazaretski *et al.*, "Design and performance of an x-ray scanning microscope at the hard x-ray nanoprobe beamline of NSLS-II," J. Synchrotron Radiat. **24**, 1113–1119 (2017).
[18]J. C. d. Silva *et al.*, "High-energy cryo x-ray nano-imaging at the ID16A beamline of ESRF," Proc. SPIE **10389**, 103890F (2017).
[19]A. Diaz *et al.*, "Three-dimensional mass density mapping of cellular ultrastructure by ptychographic x-ray nanotomography," J. Struct. Biol. **192**, 461–469 (2015).
[20]B. Pfister *et al.*, "Recreating the synthesis of starch granules in yeast," eLife **5**, e15552 (2016).
[21]S. Shahmoradian *et al.*, "Three-dimensional imaging of biological tissue by cryo x-ray ptychography," Sci. Rep. **7**, 6291 (2017).
[22]D. Liu *et al.*, "Cavitation in strained polyethylene/aluminium oxide nanocomposites," Eur. Polym. J. **87**, 255–265 (2017).
[23]L. K. H. Pallon *et al.*, "Three-dimensional nanometer features of direct current electrical trees in low-density polyethylene," Nano Lett. **17**, 1402–1408 (2017).
[24]S. Gorelick *et al.*, "High-efficiency Fresnel zone plates for hard x-rays by 100 keV e-beam lithography and electroplating," J. Synchrotron Radiat. **18**, 442–446 (2011).
[25]S. Gorelick *et al.*, "High-efficiency gold Fresnel zone plates for multi-keV x-rays," in *10th International Conference on X-Ray Microscopy*, edited by I. McNulty, C. Eyberger, and B. Lai (American Institute of Physics, Melville, 2011), Vol. 1365, pp. 88–91.
[26]Y. Hanfei, C. Ray, B. Nathalie, and S. C. Yong, "Hard x-ray nanofocusing by multilayer Laue lenses," J. Phys. D: Appl. Phys. **47**, 263001 (2014).
[27]A. Snigirev, V. Kohn, I. Snigireva, A. Souvorov, and B. Lengeler, "Focusing high-energy x rays by compound refractive lenses," Appl. Opt. **37**, 653–662 (1998).
[28]C. G. Schroer *et al.*, "High resolution imaging and lithography with hard x rays using parabolic compound refractive lenses," Rev. Sci. Instrum. **73**, 1640–1642 (2002).
[29]P. Kirkpatrick and A. V. Baez, "Formation of optical images by x-rays," J. Opt. Soc. Am. **38**, 766–774 (1948).
[30]H. Mimura *et al.*, "Breaking the 10 nm barrier in hard-x-ray focusing," Nat. Phys. **6**, 122–125 (2010).
[31]M. Holler *et al.*, "OMNY PIN—A versatile sample holder for tomographic measurements at room and cryogenic temperatures," Rev. Sci. Instrum. **88**, 113701 (2017).
[32]S. Maag *et al.*, "Development of a precision stage with delta kinematics," in euspen's 15th International Conference and Exhibition, Leuven, Belgium, 2015.
[33]M. Holler and J. Raabe, "Tracking type laser interferometer for objects with rotational degrees of freedom," patent application WO 2012079875 A1 (2010).
[34]See https://www.certif.com/ for Certified Scientific Software.
[35]See http://www.aps.anl.gov/epics/ for EPICS (Experimental Physics and Industrial Control System).
[36]M. Guizar-Sicairos *et al.*, "Phase tomography from x-ray coherent diffractive imaging projections," Opt. Express **19**, 21345–21357 (2011).
[37]M. Guizar-Sicairos *et al.*, "Quantitative interior x-ray nanotomography by a hybrid imaging technique," Optica **2**, 259–266 (2015).
[38]P. M. Pelz *et al.*, "On-the-fly scans for x-ray ptychography," Appl. Phys. Lett. **105**, 251101 (2014).
[39]J. J. Deng *et al.*, "Continuous motion scan ptychography: Characterization for increased speed in coherent x-ray imaging," Opt. Express **23**, 5438–5451 (2015).
[40]M. Odstrcil, A. Diaz, M. Holler, and M. Guizar-Sicairos, "Path toward fast, high-resolution and more photon-efficient x-ray ptychography," in *Imaging and Applied Optics 2017 (3D, AIO, COSI, IS, MATH, pcAOP) CW2B.5* (Optical Society of America, San Francisco, California, 2017).
[41]G. Ingold *et al.*, "Performance of small-gap undulators at the SLS intermediate energy storage ring," in *Synchrotron Radiation Instrumentation, Pts 1 and 2*, edited by J. Y. Choi and S. Rah (American Institute of Physics, Melville, 2007), Vol. 879, p. 388.
[42]M. Odstrčil, A. Menzel, and M. Guizar-Sicairos, "Iterative least-squares solver for generalized maximum-likelihood ptychography," Opt. Express **26**, 3108–3123 (2018).
[43]F. Zhang *et al.*, "Translation position determination in ptychographic coherent diffraction imaging," Opt. Express **21**, 13592–13606 (2013).
[44]J. Vila-Comamala *et al.*, "Dense high aspect ratio hydrogen silsesquioxane nanostructures by 100 keV electron beam lithography," Nanotechnology **21**, 285305 (2010).
[45]X. J. Huang *et al.*, "Optimization of overlap uniformness for ptychography," Opt. Express **22**, 12634–12644 (2014).
[46]P. Kraft *et al.*, "Characterization and calibration of PILATUS detectors," IEEE Trans. Nucl. Sci. **56**, 758–764 (2009).
[47]M. van Heel and M. Schatz, "Fourier shell correlation threshold criteria," J. Struct. Biol. **151**, 250–262 (2005).
[48]A. Diaz *et al.*, "Addendum to 'Three-dimensional mass density mapping of cellular ultrastructure by ptychographic x-ray nanotomography' [J. Struct. Biol. 192 (2015) 461–469]," J. Struct. Biol. **193**, 83 (2016).
[49]E. Hummel *et al.*, "3D ultrastructural organization of whole *Chlamydomonas reinhardtii* cells studied by nanoscale soft x-ray tomography," PLoS One **7**, e53293 (2012).
[50]J. J. Deng *et al.*, "X-ray ptychographic and fluorescence microscopy of frozen-hydrated cells using continuous scanning," Sci. Rep. **7**, 445 (2017).